The Journal of Chemical Physics ARTICLE scitation.org/journal/jcp

Ultrafast charge carrier dynamics in quantum confined 2D perovskite

Cite as: J. Chem. Phys. 152, 214705 (2020); doi: 10.1063/5.0008608
Submitted: 23 March 2020 • Accepted: 13 May 2020 •
Published Online: 3 June 2020

Giulia Folpini,[1] Lorenzo Gatto,[2,3] Daniele Cortecchia,[1] Michele Devetta,[2] Gabriele Crippa,[2,3] Caterina Vozzi,[2] Salvatore Stagira,[2,3,a)] Annamaria Petrozza,[1] and Eugenio Cinquanta[2,a)]

AFFILIATIONS

[1]Center for Nano Science and Technology, Istituto Italiano di Tecnologia, Milano, Italy
[2]Istituto di Fotonica e Nanotecnologie, Consiglio Nazionale delle Ricerche, Milano, Italy
[3]Dipartimento di Fisica, Politecnico di Milano, Milano, Italy

[a)]**Authors to whom correspondence should be addressed:** salvatore.stagira@polimi.it and eugenioluigi.cinquanta@cnr.it

ABSTRACT

We studied the charge carrier dynamics in 2D perovskite NBT_2PbI_4 by ultrafast optical pump–THz probe spectroscopy. We observed a few ps long relaxation dynamics that can be ascribed to the band to band carrier recombination, in the absence of any contribution from many-body and trap assisted processes. The transient conductivity spectra show that the polaron dynamics is strongly modulated by the presence of a rich exciton population. The polarization field resulting from the exciton formation acts as the source of a restoring force that localizes polarons. This is revealed by the presence of a negative imaginary conductivity. Our results show that the dynamics of excitons in 2D perovskites at room temperature can be detected by monitoring their effect on the conductivity of the photoinduced polaronic carrier.

INTRODUCTION

In recent years, metal-halide perovskites have garnered considerable interest because of their promising qualities for photovoltaics and light-emitting applications.[1–3] Perovskites with a large organic cation assembled in two-dimensional (2D) structures, with layers of inorganic Pb–I octahedra alternated with layers of organic cations, are particularly attractive as light-emitting diodes and active lasing materials.[4–6] Due to the quantum and electronic confinement in the single layer, the exciton binding energy is in the order of 200–300 meV, hence promoting excitons as the primary products of the photoexcitation.[7–12] This exciton population has been, for instance, considered for broad sub-bandgap emission in some materials, both at room and low temperatures.[13–18] The soft lattice with the related polaronic nature of the carriers, combined with the presence of excitons, makes the photophysical properties extremely peculiar.[18–22] The interplay between the primary photoexcited unbound carriers, excitons, and response of the lattice has not been fully revealed so far, making the transport properties and recombination dynamics of quantum confined perovskites still elusive.

Ultrafast THz spectroscopy is a powerful technique sensitive to free carriers and lattice excitation. Indeed, THz photoconductivity is affected by polar phonons, excited species that are both charged and mobile, and exciton related phenomena.[23] Concerning bound electron–hole pairs, ultrafast THz spectroscopy is sensitive to charged excitons, i.e., trions, and intra-excitonic transitions, as demonstrated, for instance, in the 2D material MoS_2 and in organometal halide perovskites, respectively.[24,25] Although for the 2D perovskites, the photoexcitation creates an exciton population that largely exceeds the free carriers one,[12] the presence of the exciton bath has a sizable impact on the minority unbound electron–hole pairs by modifying the dielectric landscape within the 2D layer.

In this work, we exploit terahertz time-domain spectroscopy in the optical pump–THz probe (OPTP) scheme to study the dynamics of photo-generated carriers in a prototypical 2D perovskite. We choose n-butylammonium lead iodide $(NBT)_2PbI_4$ as a prototypical material characterized by a strong green emission. This material has been already exploited for photovoltaics applications, lasing, and development of LED devices, showing light-emitting efficiencies of

the order of 1% and prominent amplified spontaneous emission at room temperature.[26–28]

METHODS

We performed OPTP spectroscopy exploiting our terahertz time-domain spectrometer driven by 25-fs pulses from a 1-kHz Ti:sapphire laser with a central wavelength of 790 nm (1.6 eV). THz pulses with a 0.1–2.7 THz bandwidth were generated and detected by electro-optic sampling in two 1-mm thick ZnTe crystals. A fraction of the Near-Infrared (NIR) 25 fs pump is used as a gate for electro-optic sampling: the electro-optic sampling time t_{eos} is defined as the delay between the gate and the THz electric field, with $t_{eos} = 0$ corresponding to the maximum of the THz electric field waveform. For the excitation of the sample, 400-nm (3.1 eV), 100-fs laser pulses were focused on a spot size diameter of 3 mm at fluences of 25 $\mu J\ cm^{-2}$, 50 $\mu J\ cm^{-2}$, and 65 $\mu J\ cm^{-2}$ with a corresponding photoexcitation density of $3 \cdot 10^{17}$–$7 \cdot 10^{17}\ cm^{-3}$. Purging with N_2 was used to remove water vapor from the THz beam path.

RESULTS

The crystal structure of NBT_2PbI_4 is shown in Fig. 1(a). The PbI_4 octahedrals are separated by the large organic cations with a spacing of 8.7 nm, arranged along the ⟨100⟩ orientation.[14] The material was spin-coated to obtain 500 nm thin films on 1 mm thick fused silica substrates. The chosen film thickness allows for the detection of THz transient photoconductivity even at relatively low photoexcitation density. However, it also results in higher structural disorder in the polycrystalline film. X-ray diffraction measurements (Fig. S1) on thin films showed a single strong diffraction peak, corresponding to the predominant orientation of crystalline planes. The absence of additional peaks shows that the 2D crystalline planes are stacked in the same direction. However, the width of the diffraction peak increases from 0.3° in a 100 nm thick film to 0.5° in a 500 nm thick film, corresponding to crystallites of 40–50 nm inside the grains of the thin film.

The excitonic peak in the absorbance [in blue, left scale, Fig. 1(b)] is broad and appears to be composed of multiple bands centered at 495 nm, 518 nm, and 550 nm. This peculiar shape generally appears for thicker films (e.g., >150 nm) for buthylammine based 2D perovskites:[29] this deviation from the sharper excitonic peak found in thinner films stems from an increase in disorder in thick films together with saturation of available absorption centers.

The photoluminescence (PL) emission of NBT_2PbI_4 is centered at 519 nm [Fig. 1(b), in green], with a FWHM of 22 nm. A strong asymmetry is visible, due to a negligible Stokes shift, together with the appearance of small shoulders. The emission comes from exciton recombination, as confirmed by the linearity of PL intensity with the pump fluence.[14] We show the photoluminescence dynamics of the excitonic peak [integrated over a range from 480 nm to 600 nm, Fig. 1(c)] in a temporal window of 1 ns: the luminescence decay can be fitted with a stretched exponential function[30] $I(t) = I_0 e^{-\left(\frac{t}{\tau_0}\right)^{\beta}}$ with an average population lifetime $\tau_0 = 70$ ps and a stretch factor $\beta = 0.76$. A stretch factor $\beta < 1$ indicates that the PL decay is not very well described by a single decay rate but rather by a distribution,[31] stemming from inhomogeneity in the spatial and energetic landscape explored by the photocarriers. For comparison, in thinner samples (e.g., 200 nm, see Fig. S2), the luminescence decay can be fitted with a stretch factor close to one ($\beta = 0.81$); thus, the disorder seems to be correlated with the presence of numerous smaller crystallites in the thin film.

In order to investigate the photophysics of this material, we first characterized the optical properties of the unexcited NBT_2PbI_4 thin film in the THz spectral domain. To retrieve the complex refractive index of the film from its complex THz transmission, we followed the procedure reported in Ref. 32 and we extracted the related error bars, as reported in Ref. 33. Figure 2(a) shows the real part $n(\omega)$ of the complex refractive index as extracted by the optimization process. The inflection points observed for n correspond to the peaks of the THz absorption spectrum of the sample reported in Fig. 2(b). The comparison with the IR active modes and related cross sections calculated by Thouin *et al.*[22] allowed us to attribute the observed features in the complex refractive index to anharmonic and polar bending and mixed stretching/bending modes of the soft NBT_2PbI_4 lattice, as also observed for 3D lead halide perovskites.[32–36]

For exploring the carrier dynamics, we studied the transient change in the THz field at the peak of the pulse as a function of the pump–probe delay.[37] Figure 3 reports the relative transient electric field change $-\frac{\Delta E(tp,t_{eos})}{E0}$ in correspondence with the peak of the THz waveform in the time domain ($t_{eos} = 0$), at pump fluences of 25 $\mu J\ cm^{-2}$, 50 $\mu J\ cm^{-2}$, and 65 $\mu J\ cm^{-2}$. Here, $\Delta E(t_p,0)$ is the change in the transmitted THz field detected at different pump–probe delays t_p and $E_0 = E(0)$ is the maximum of the THz field transmitted by the unexcited sample.

In contrast with the dynamics reported for 3D perovskites, we observed a buildup of the signal within the instrument response

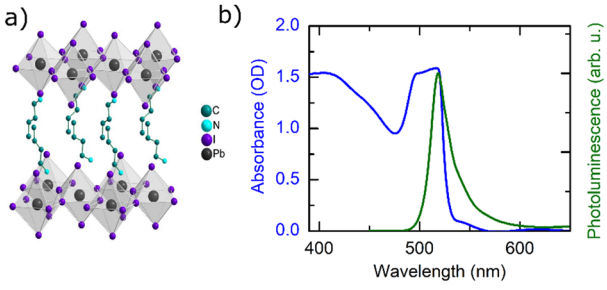

FIG. 1. (a) Schematic NBT_2PbI_4 structure. (b) Optical characterization of a 500 nm thick NBT_2PbI_4 thin film (full lines): absorbance (in blue) and PL emission (in green). (c) Lifetime of the PL emission integrated between 480 nm and 600 nm under optical pumping at 400 nm.

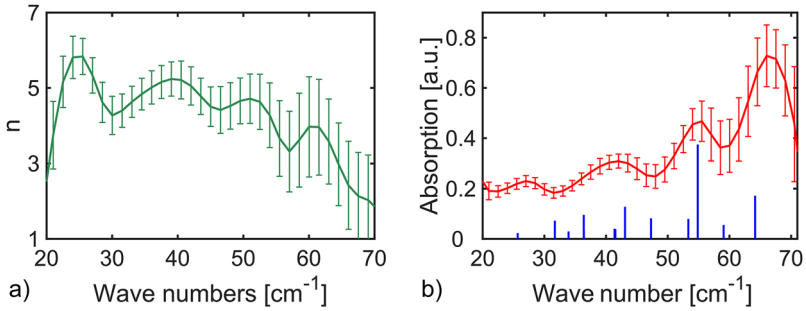

FIG. 2. Static complex refractive index of $NBT_2Pb_2I_4$. (a) Real part of the refractive index. (b) THz absorption spectrum (red continuous line) and calculated IR active phonon together with their cross sections (blue vertical continuous line). The experimental spectrum has been vertically stacked for clarity.

function (IRF) followed by an ultrafast recovery on the few-ps time scale.[32,38,39] Recently, Kumar *et al.* obtained a similar result by studying confined perovskites and fitted the observed dynamics with biexponential decay functions. They attributed the observed decay times to carrier cooling via el-ph scattering and band to band recombination.[40] We made a global fit of the normalized $-\frac{\Delta E(tp,0)}{E0}$ dynamics with the following rate equation:

$$\frac{dn(t)}{dt} = -k_2 n^2(t), \tag{1}$$

where $n(t)$ is the carrier density and k_2 is the bimolecular decay rate. We chose Eq. (1) because the more general rate equation that considers monomolecular and Auger recombination returns a negligible contribution for the corresponding decay rate k_1 and k_3.[41] We extracted $k_2 \sim 5 \cdot 10^{-9}$ cm^3 s^{-1} and attributed the observed dynamics to the recombination of the minority unbound photoinjected charges that do not contribute to the sub-ps formation of excitons.[21] The absence of many-body processes in the recombination dynamics is compatible with the relatively low excitation density of ~10^{17} *carriers* cm^{-3}. The negligible trap-assisted recombination we observed, which typically occurs at much longer time scales (ns and μs), can be ascribed to the quantum confinement that limits the transport in the 2D single layer and makes the carrier recombination much faster than the trap-assisted one.

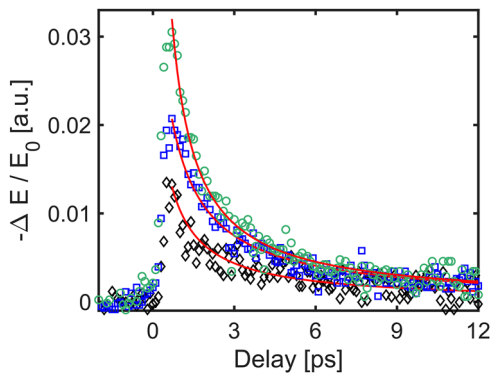

FIG. 3. Charge carrier dynamics of the 2D perovskite thin film. $-\Delta E/E_0$ observed at 25 μJ cm^{-2} (black diamonds), 50 μJ cm^{-2} (blue squares), and 65 μJ cm^{-2} (green circles); the red curve is the related fit to rate equation (1).

Then, we analyzed the transient conductivity spectra of the $NBT_2Pb_2I_4$ perovskite thin films by sampling the entire waveform of the THz electric field and different pump–probe delays. This approach allowed us to obtain the pump induced frequency-resolved complex dielectric response, which offers further insight into the rich charge carrier dynamics occurring during the first few ps after excitation. Figure 4(a) shows the real $\Delta\sigma_1(\omega,\tau)$ and the imaginary $\Delta\sigma_2(\omega,\tau)$ part of the optical conductivity obtained at a fluence of 65 μJ cm^{-2} at 0.5 ps after the photoexcitation. First, we observe the presence of peaks in $\Delta\sigma_1(\omega,\tau)$ accompanied by inflection points in $\Delta\sigma_2(\omega,\tau)$ at the same energy around 30 cm^{-1}, 40 cm^{-1}, 55 cm^{-1}, and 65 cm^{-1}, slightly shifted with respect to the peaks observed in the absorption spectrum of the unexcited sample (Fig. 2). These spectral features are the distinctive signatures of the presence of polaronic carriers. Indeed, they reflect the coupling of the photoinjected charges with the phonons of the soft lattice deformed by the photoexcitation, as already demonstrated for 3D perovskites.[32] Figure 4(b) shows that the polaronic fingerprints appear also at lower fluencies (25 μJ cm^{-2} and 50 μJ cm^{-2}), confirming the robustness of our observations. More intriguingly, $\Delta\sigma_1(\omega,\tau)$ vanishes for $\omega \to 0$ and monotonically grows with the increase in frequency $[\frac{d(\Delta\sigma_1(\omega,\tau))}{d\omega} > 0]$, while $\Delta\sigma_2(\omega,\tau)$ is negative at all frequency. This evidences the presence of a restoring force acting on the polaronic carriers. As implemented for other low dimensional materials,[42–44] we fit the observed transient THz conductivity with a Drude–Lorentz model,

$$\Delta\sigma(\omega) = \frac{n_f q^2 \tau}{m^*(1 - \iota\omega\tau)} + \frac{\iota\omega F_0}{\left(\omega_0^2 - \omega^2\right) + \iota\Gamma_0\omega}, \tag{2}$$

where in the first (Drude) term, q, m^*, n_f, and τ are the charge, effective mass, density, and scattering time of the carriers, while in the second (Lorentz) term, F_0, ω_0, and Γ_0 are the strength central frequency and width of the oscillator. Figures 4(c)–4(f) show the fit with Eq. (2) of the complex photoconductivity at 0.5 ps, 1 ps, 2 ps, and 4 ps after the photoexcitation, respectively. As for the case of 1D and 2D confined materials,[42–44] the Drude–Lorentz model qualitatively reproduces the dispersion of the optical conductivity. The positive and increasing $\Delta\sigma_1(\omega,\tau)$ reflects the response of charged carriers, while the negative $\Delta\sigma_2(\omega,\tau)$ points to the localization of such carriers. The observed conductivity stems from the response of charged polarons and cannot be directly connected to the presence of two distinct populations of unbound and bound carriers (Drude and Lorentz terms, respectively). First of

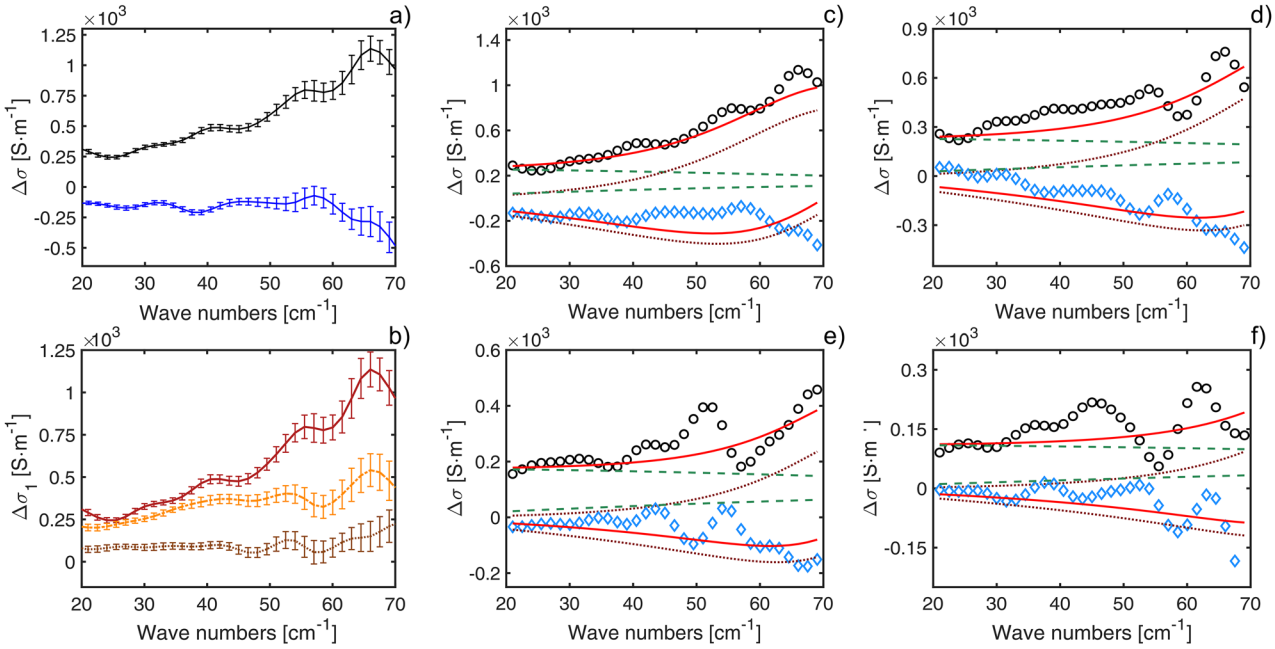

FIG. 4. Photoinduced complex optical conductivity of the 2D perovskite thin film. (a) Real $\Delta\sigma_1$ (black line) and imaginary $\Delta\sigma_2$ part (blue line) of the optical conductivity acquired at 65 μJ cm^{-2} 0.5 ps after the photoexcitation; (b) $\Delta\sigma_1$ acquired 0.5 ps after the photoexcitation at 28 (maroon dotted curve), 50 (yellow dashed-dotted curve), and 65 μJ cm^{-2} (red continuous curve); [(c)–(f)] $\Delta\sigma_1$ (black empty circles) and $\Delta\sigma_2$ (blue empty diamonds) acquired at 65 μJ cm^{-2} for 0.5 ps, 1 ps, 2 ps, and 4 ps pump-probe delays, respectively, together with the related Drude–Lorenz fit (red continuous curve). The green dashed curve and maroon dotted curve are the Drude and Lorentz contribution to the fit, respectively.

all, the dynamics reported in Fig. 3 can be sharply fitted by a rate equation, which considers the presence of one species only. Furthermore, we can be directly sensitive neither to the inter-exciton transition at ~300 cm^{-1}, observed in 2D perovskites using visible pump–probe spectroscopy,[21] nor to exciton resonances that typically occur at PHz frequencies. Finally, THz radiation has been proved to be sensitive to intra-excitonic transition in organometal halide perovskite and Quantum Wells (QWs) of GaAs.[25,45] For the observation of those transitions, the samples were kept at cryogenic temperature to avoid exciton ionization, and for the QW case, resonant pumping was mandatory to observe the intra-exciton transition. Since we are not resonantly pumping the excitons and our measurements are performed at room temperature, the contribution of intra-exciton transition to the optical conductivity of the NBT_2PbI_4 thin film can be excluded. As a consequence, the response to the photoexcitation measured by the THz probe must be related to the charged polaronic carriers only. As no external field has been applied to the sample during the measurement, the localization must be due to the electrostatic force originated by a microscopic field inside the material. In this respect, the presence of excitons in the single layer of PEA_2PbI_4 and $NBT_2Pb_2I_4$ 2D perovskites has already been demonstrated[21,22] and can explain the origin of the observed conductivity. Indeed, excitons can be viewed as an ensemble of interacting dipoles, which are the source of a polarization field. The resulting force acts on the polaronic carriers inducing their localization in the 2D layer and the consequent negative $\Delta\sigma_2(\omega,\tau)$.[44,46,47]

To extract the mobility of the polaronic carriers from the Drude term of the fit function, we adopt the *el* and *h* effective masses reported in the literature for the $(PEA)_2PbI_4$ case, by multiplying the reported values by a factor of 3 to consider the effect of the lattice on the carrier masses.[48] We obtain μ ~ 10–70 cm^2 V^{-1} s^{-1}, compatible with the results extracted for different 2D perovskites using THz and microwave spectroscopy.[49] Concerning the Lorentzian contribution, the exciton population evolves via inter-exciton transitions up to hundreds of ps and its contribution to the optical conductivity can be detected as long as the small amount of unbound polaronic carriers does not recombine. The snapshot of the excited system evidences that a small population of the photoinjected hot carriers forms polarons and does not further bind to form excitons, being hence detectable by the THz probe.

CONCLUSION

We exploited ultrafast THz spectroscopy to explore the dynamics of the photocarrier population in the prototypical 2D perovskite NBT_2PbI_4. We observed a recovery of the THz transient signal within a few ps after the photoexcitation that can be assigned to the band to band carrier recombination. From the analysis of the THz complex conductivity spectra, we confirm the presence of a small amount of unpaired polaronic carriers diluted in a large excitonic bath. To address the polaronic character of excitons, i.e., exciton-polarons, a computational model and further experimental efforts, for instance, as a function of the

temperature and the number of stacked 2D perovskite layers, are required.

SUPPLEMENTARY MATERIAL

See the supplementary material for details about the sample preparation, optical characterization, and extraction of the optical conductivity from the raw THz data.

ACKNOWLEDGMENTS

This study was supported by Ministero dell'Istruzione, dell'Università e della Ricerca (MIUR), with the ELI project ESFRI Roadmap; by Regione Lombardia through the projects "Cyber-Sort"; and by the European Research Council Starting Research Grant UDYNI (Grant No. 307964).

DATA AVAILABILITY

The data that support the findings of this study are available from the corresponding author upon reasonable request.

REFERENCES

[1] T. Leijtens, K. A. Bush, R. Prasanna, and M. D. McGehee, Nat. Energy **3**, 828 (2018).
[2] K. Lin, J. Xing, L. N. Quan, F. P. G. de Arquer, X. Gong, J. Lu, L. Xie, W. Zhao, D. Zhang, C. Yan, W. Li, X. Liu, Y. Lu, J. Kirman, E. H. Sargent, Q. Xiong, and Z. Wei, Nature **562**, 245 (2018).
[3] Y. Cao, N. Wang, H. Tian, J. Guo, Y. Wei, H. Chen, Y. Miao, W. Zou, K. Pan, Y. He, H. Cao, Y. Ke, M. Xu, Y. Wang, M. Yang, K. Du, Z. Fu, D. Kong, D. Dai, Y. Jin, G. Li, H. Li, Q. Peng, J. Wang, and W. Huang, Nature **562**, 249 (2018).
[4] G. Grancini and M. K. Nazeeruddin, Nat. Rev. Mater. **4**, 4 (2019).
[5] B. R. Sutherland and E. H. Sargent, Nat. Photonics **10**, 295 (2016).
[6] S. Adjokatse, H.-H. Fang, and M. A. Loi, Mater. Today **20**, 413 (2017).
[7] T. Ishihara, J. Takahashi, and T. Goto, Phys. Rev. B **42**, 11099 (1990).
[8] J. Even, L. Pedesseau, and C. Katan, ChemPhysChem **15**, 3733 (2014).
[9] B. Saparov and D. B. Mitzi, Chem. Rev. **116**, 4558 (2016).
[10] K. Gauthron, J.-S. Lauret, L. Doyennette, G. Lanty, A. Al Choueiry, S. J. Zhang, A. Brehier, L. Largeau, O. Mauguin, J. Bloch, and E. Deleporte, Opt. Express **18**, 5912–5919 (2010).
[11] C. Katan, N. Mercier, and J. Even, Chem. Rev. **119**, 3140 (2019).
[12] D. Marongiu, M. Saba, F. Quochi, A. Mura, and G. Bongiovanni, J. Mater. Chem. C **7**, 12006 (2019).
[13] D. Cortecchia, J. Yin, A. Petrozza, and C. Soci, J. Mater. Chem. C **7**, 4956 (2019).
[14] D. Cortecchia, S. Neutzner, A. R. Srimath Kandada, E. Mosconi, D. Meggiolaro, F. De Angelis, C. Soci, and A. Petrozza, J. Am. Chem. Soc. **139**, 39 (2017).
[15] M. D. Smith and H. I. Karunadasa, Acc. Chem. Res. **51**, 619 (2018).
[16] J. Luo, X. Wang, S. Li, J. Liu, Y. Guo, G. Niu, L. Yao, Y. Fu, L. Gao, Q. Dong, C. Zhao, M. Leng, F. Ma, W. Liang, L. Wang, S. Jin, J. Han, L. Zhang, J. Etheridge, J. Wang, Y. Yan, E. H. Sargent, and J. Tang, Nature **563**, 541 (2018).
[17] E. R. Dohner, A. Jaffe, L. R. Bradshaw, and H. I. Karunadasa, J. Am. Chem. Soc. **136**, 13154 (2014).
[18] X. Wang, W. Meng, W. Liao, J. Wang, R.-G. Xiong, and Y. Yan, J. Phys. Chem. Lett. **10**, 501 (2019).
[19] S. Neutzner, F. Thouin, D. Cortecchia, A. Petrozza, C. Silva, and A. R. Srimath Kandada, Phys. Rev. Mater. **2**, 064605 (2018).
[20] F. Thouin, S. Neutzner, D. Cortecchia, V. A. Dragomir, C. Soci, T. Salim, Y. M. Lam, R. Leonelli, A. Petrozza, A. R. S. Kandada, and C. Silva, Phys. Rev. Mater. **2**, 034001 (2018).
[21] F. Thouin, A. R. Srimath Kandada, D. A. Valverde-Chávez, D. Cortecchia, I. Bargigia, A. Petrozza, X. Yang, E. R. Bittner, and C. Silva, Chem. Mater. **31**, 7085 (2019).
[22] F. Thouin, D. A. Valverde-Chávez, C. Quarti, D. Cortecchia, I. Bargigia, D. Beljonne, A. Petrozza, C. Silva, and A. R. Srimath Kandada, Nat. Mater. **18**, 349 (2019).
[23] R. Ulbricht, E. Hendry, J. Shan, T. F. Heinz, and M. Bonn, Rev. Mod. Phys. **83**, 543 (2011).
[24] C. H. Lui, A. J. Frenzel, D. V. Pilon, Y.-H. Lee, X. Ling, G. M. Akselrod, J. Kong, and N. Gedik, Phys. Rev. Lett. **113**, 166801 (2014).
[25] L. Luo, L. Men, Z. Liu, Y. Mudryk, X. Zhao, Y. Yao, J. M. Park, R. Shinar, J. Shinar, K.-M. Ho, I. E. Perakis, J. Vela, and J. Wang, Nat. Commun. **8**, 15565 (2017).
[26] H. Tsai, W. Nie, J.-C. Blancon, C. C. Stoumpos, R. Asadpour, B. Harutyunyan, A. J. Neukirch, R. Verduzco, J. J. Crochet, S. Tretiak, L. Pedesseau, J. Even, M. A. Alam, G. Gupta, J. Lou, P. M. Ajayan, M. J. Bedzyk, M. G. Kanatzidis, and A. D. Mohite, Nature **536**, 312 (2016).
[27] C. M. Raghavan, T.-P. Chen, S.-S. Li, W.-L. Chen, C.-Y. Lo, Y.-M. Liao, G. Haider, C.-C. Lin, C.-C. Chen, R. Sankar, Y.-M. Chang, F.-C. Chou, and C.-W. Chen, Nano Lett. **18**, 3221 (2018).
[28] H. Hu, T. Salim, B. Chen, and Y. M. Lam, Sci. Rep. **6**, 33546 (2016).
[29] J.-F. Liao, H.-S. Rao, B.-X. Chen, D.-B. Kuang, and C.-Y. Su, J. Mater. Chem. A **5**, 2066 (2017).
[30] M. N. Berberan-Santos, E. N. Bodunov, and B. Valeur, Chem. Phys. **315**, 171 (2005).
[31] M. N. Berberan-Santos and B. Valeur, J. Lumin. **126**, 263 (2007).
[32] E. Cinquanta, D. Meggiolaro, S. G. Motti, M. Gandini, M. J. P. Alcocer, Q. A. Akkerman, C. Vozzi, L. Manna, F. De Angelis, A. Petrozza, and S. Stagira, Phys. Rev. Lett. **122**, 166601 (2019).
[33] M. Karakus, S. A. Jensen, F. D'Angelo, D. Turchinovich, M. Bonn, and E. Cánovas, J. Phys. Chem. Lett. **6**(24), 4991–4996 (2015).
[34] C. La-o-vorakiat, H. Xia, J. Kadro, T. Salim, D. Zhao, T. Ahmed, Y. M. Lam, J.-X. Zhu, R. A. Marcus, M.-E. Michel-Beyerle, and E. E. M. Chia, J. Phys. Chem. Lett. **7**, 1 (2016).
[35] D. Zhao, J. M. Skelton, H. Hu, C. La-o-vorakiat, J. X. Zhu, R. A. Marcus, M. E. Michel-Beyerle, Y. M. Lam, A. Walsh, and E. E. M. Chia, Appl. Phys. Lett. **111**, 201903 (2017).
[36] M. Nagai, T. Tomioka, M. Ashida, M. Hoyano, R. Akashi, Y. Yamada, T. Aharen, and Y. Kanemitsu, Phys. Rev. Lett. **121**, 145506 (2018).
[37] M. C. Beard, G. M. Turner, and C. A. Schmuttenmaer, J. Phys. Chem. B **106**, 7146 (2002).
[38] M. B. Johnston and L. M. Herz, Acc. Chem. Res. **49**, 146–154 (2016).
[39] S. A. Bretschneider, I. Ivanov, H. I. Wang, K. Miyata, X. Zhu, and M. Bonn, Adv. Mater. **30**, 1707312 (2018).
[40] A. Kumar, A. Solanki, M. Manjappa, S. Ramesh, Y. K. Srivastava, P. Agarwal, T. C. Sum, and R. Singh, Sci. Adv. **6**, eaax8821 (2020).
[41] C. Wehrenfennig, G. E. Eperon, M. B. Johnston, H. J. Snaith, and L. M. Herz, Adv. Mater. **26**(10), 1584–1589 (2014).
[42] M. C. Beard, J. L. Blackburn, and M. J. Heben, Nano Lett. **8**(12), 4238–4242 (2008).
[43] C. J. Docherty, P. Parkinson, H. J. Joyce, M.-H. Chiu, C.-H. Chen, M.-Y. Lee, L.-J. Li, L. M. Herz, and M. B. Johnston, ACS Nano **8**(11), 11147–11153 (2014).
[44] X. Xing, L. Zhao, Z. Zhang, X. Liu, K. Zhang, Y. Yu, X. Lin, H. Y. Chen, J. Q. Chen, Z. Jin, J. Xu, and G.-h. Ma, J. Phys. Chem. C **121**, 20451–20457 (2017).
[45] R. A. Kaindl, D. Hägele, M. A. Carnahan, and D. S. Chemla, Phys. Rev. B **79**, 045320 (2009).
[46] J. J. Hopfield, Phys. Rev. **112**, 1555 (1958).
[47] J. L. Hughes and T.-I. Jeon, J. Infrared Milli Terahz Waves **33**, 871–925 (2012).
[48] Y.-Q. Zhao, Q.-R. Ma, B. Liu, Z.-L. Yu, J. Yang, and M.-Q. Cai, Nanoscale **10**, 8677–8688 (2018).
[49] N. T. P. Hartono, S. Sun, M. C. Gélvez-Rueda, P. J. Pierone, M. P. Erodici, J. Yoo, F. Wei, M. Bawendi, F. C. Grozema, M.-j. Sher, T. Buonassisi, and J.-P. Correa-Baena, J. Mater. Chem. A **7**, 23949 (2019).